Atmos. Chem. Phys., 13, 9447–9459, 2013
www.atmos-chem-phys.net/13/9447/2013/
doi:10.5194/acp-13-9447-2013

Atmospheric Chemistry and Physics Open Access

The covariation of Northern Hemisphere summertime CO_2 with surface temperature in boreal regions

D. Wunch[1], P. O. Wennberg[1], J. Messerschmidt[1], N. C. Parazoo[2,3], G. C. Toon[1,2], N. M. Deutscher[4], G. Keppel-Aleks[5], C. M. Roehl[1], J. T. Randerson[5], T. Warneke[4], and J. Notholt[4]

[1]California Institute of Technology, Pasadena, CA, USA
[2]Jet Propulsion Laboratory, California Institute of Technology, Pasadena, CA, USA
[3]Joint Institute for Regional Earth System Science and Engineering, University of California, Los Angeles, CA, USA
[4]University of Bremen, Bremen, Germany
[5]Department of Earth System Science, University of California, Irvine, CA, USA

Correspondence to: D. Wunch (dwunch@gps.caltech.edu)

Received: 12 March 2013 – Published in Atmos. Chem. Phys. Discuss.: 19 April 2013
Revised: 26 July 2013 – Accepted: 12 August 2013 – Published: 26 September 2013

Abstract. We observe significant interannual variability in the strength of the seasonal cycle drawdown in northern midlatitudes from measurements of CO_2 made by the Total Carbon Column Observing Network (TCCON) and the Greenhouse Gases Observing Satellite (GOSAT). This variability correlates with surface temperature in the boreal regions. Using TCCON measurements, we find that the slope of the relationship between the X_{CO_2} seasonal cycle minima and boreal surface temperature is 1.2 ± 0.7 ppm K^{-1}. Assimilations from CarbonTracker 2011 and CO_2 simulations using the Simple Biosphere exchange Model (SiB) transported by GEOS-Chem underestimate this covariation. Both atmospheric transport and biospheric activity contribute to the observed covariation.

1 Introduction

Fossil fuel burning, the oceans, and the global terrestrial biosphere control the atmospheric concentrations and variability of carbon dioxide (CO_2). On interannual timescales, variations in fluxes from terrestrial ecosystems, driven by changes in surface temperature and precipitation, are the dominant drivers of variability in atmospheric CO_2 (Francey et al., 1995; Langenfelds et al., 2002; Rayner et al., 1999; Welp et al., 2011; Cox et al., 2013). On these timescales, warm years tend to be associated with more rapid increases in atmospheric CO_2, and cool years with reduced growth rates (Braswell et al., 1997). This positive relationship between temperature and atmospheric CO_2 is attributed primarily to an increase in ecosystem respiration (R_e) with increasing surface temperature, and a concurrently muted gross primary production (GPP, or photosynthesis) (Doughty and Goulden, 2008).

The shape of the seasonal cycle in atmospheric CO_2 in the northern midlatitudes is primarily determined by the seasonal imbalance between R_e and GPP (Randerson et al., 1997; Messerschmidt et al., 2013), which is referred to as net ecosystem exchange (NEE), where positive NEE is defined here as a net flux of CO_2 into the atmosphere. At high latitudes, there is a significant time lag between GPP and R_e: GPP peaks around the summer solstice when photosynthesis is at a seasonal maximum, whereas R_e peaks later in summer when air and ground temperatures are warmest. This creates a negative NEE during the growing season (June, July and August) (Lloyd and Taylor, 1994). The growing season NEE has the largest magnitude over the temperate and boreal forest region of the Northern Hemisphere (Fung et al., 1987), producing the observed seasonal cycle in northern midlatitude CO_2 (Machta, 1972, and Fig. 1). The seasonal cycles at all northern midlatitudes are highly sensitive to changes in the NEE in the boreal forests (D'Arrigo et al., 1987; Randerson et al., 1997; Keppel-Aleks et al., 2011), where there is also significant temperature-driven variability (Randerson et al., 1999; Piao et al., 2008). Thus, the atmospheric seasonal cycle and its variability can provide insight into the response

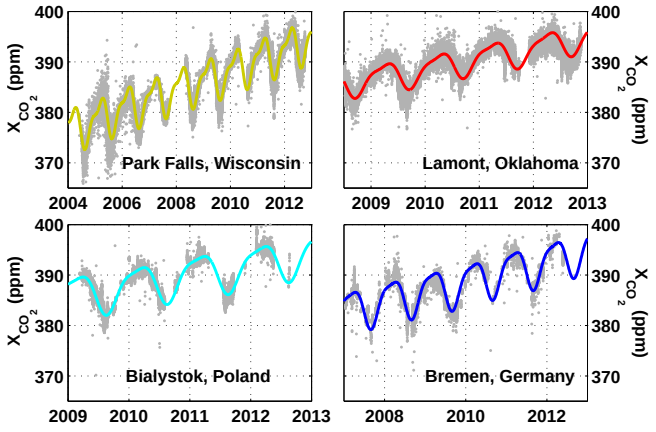

Fig. 1. The time series of X_{CO_2} measured at four Northern Hemisphere TCCON stations. The solid lines are the periodic fits to the time series.

of carbon pools to climate (Keeling et al., 1996; Randerson et al., 1997).

Previous analyses of the role of temperature on atmospheric CO_2 have relied on highly precise and accurate atmospheric CO_2 concentrations or fluxes measured by surface or near-surface in situ instruments located throughout the world. Tower flux measurements have shown a strong sensitivity of carbon exchange to surface temperature at several locations, including Niwot Ridge, Colorado (Sacks et al., 2007), Howland Forest, Maine (Richardson et al., 2007), and in the North American prairie region (Arnone et al., 2008). In this paper, we use measurements of column-averaged dry-air mole fractions of CO_2, denoted X_{CO_2}, from the Total Carbon Column Observing Network (TCCON, Wunch et al., 2011a) and from the Greenhouse Gases Observing Satellite (GOSAT, Hamazaki, 2005; Yokota et al., 2009) to examine the interannual variability of the seasonal cycle minimum and its relationship with surface temperature. Compared with surface in situ measurements of CO_2 mole fractions, X_{CO_2} is influenced much less by planetary boundary layer height changes, and possesses a much larger spatial sensitivity footprint (on the order of hundreds to thousands of kilometers, Keppel-Aleks et al., 2011). The north–south gradients in X_{CO_2} in the Northern Hemisphere summertime are large, and hence the latitudinal origin of the measured air parcel strongly influences its X_{CO_2} (Keppel-Aleks et al., 2012).

There have been marked interannual differences in the seasonal cycle minima of X_{CO_2} in the Northern Hemisphere in recent years (Figs. 1, 2). Guerlet et al. (2013) have also described significant differences in the 2009 and 2010 seasonal cycle amplitudes using the GOSAT data. These interannual differences are sometimes underestimated in Earth system models, which explicitly represent feedbacks between climate and terrestrial carbon fluxes (Keppel-Aleks et al., 2013).

We find that the measured X_{CO_2} seasonal cycle minima are positively correlated with the measured surface temperature anomalies in boreal regions. Using atmospheric total column measurements, the CarbonTracker assimilation output (CarbonTracker, 2011) and global CO_2 simulations using the Simple Biosphere model (Sellers et al., 1996a), we investigate the following processes for their contribution to the observed interannual variability in X_{CO_2}: the relative contributions of fire, fossil fuel, terrestrial biosphere, and ocean fluxes, and dynamical drivers of interannual variability.

In the following sections, we describe the data and model sources, and outline our analysis methods. We then discuss the results of the analyses.

2 TCCON

The TCCON is composed of ground-based Fourier transform spectrometers distributed throughout the world that provide measurements of X_{CO_2} (Wunch et al., 2011a). We use data from the four longest-running Northern Hemisphere TCCON sites: Park Falls, Wisconsin, USA (46° N, 90° W, Washenfelder et al., 2006); Lamont, Oklahoma, USA (37° N, 97° W); Białystok, Poland (53° N, 23° E, Messerschmidt et al., 2012); and Bremen, Germany (53° N, 9° E). In Bremen, the construction of the solar tracker was completed in 2006, so we include measurements from the beginning of the subsequent calendar year. The X_{CO_2} values from these four sites have been tied to the World Meteorological Office scale through comparisons with aircraft profiles (Washenfelder et al., 2006; Wunch et al., 2010; Messerschmidt et al., 2011). We use the GGG2012 version of the TCCON data, available from http://tccon.ipac.caltech.edu, applying the corrections to Park Falls (+0.8 ppm after 23 June 2011) and Lamont (−0.5 ppm after 14 April 2011) recommended on the TCCON data description webpage: https://tccon-wiki.caltech.edu/Network_Policy/Data_Use_Policy/Data_Description.

3 GOSAT

The GOSAT satellite, carrying the Thermal and Near-Infrared Sensor for carbon Observation Fourier transform spectrometer (TANSO-FTS), was launched in January 2009 and has a ground-repeat cycle of 3 days and a footprint size of approximately 100 km^2 (Yokota et al., 2009; Crisp et al., 2012). We use the X_{CO_2} derived from GOSAT spectra by the Atmospheric CO_2 Observations from Space (ACOS) build 3.3 retrieval algorithm (Crisp et al., 2012; O'Dell et al., 2012). Data from 1 April 2009 through 13 April 2013 are used in this study. The data were filtered and corrected for retrieval biases using the method described in the ACOS Level 2 Standard Product Data Users Guide, v3.3, available from http://disc.sci.gsfc.nasa.gov/datareleases/acos-version-3.3.

We define GOSAT-TCCON coincidences in the same manner as Wunch et al. (2011b). We use relatively wide latitude (±5°), longitude (±30°) and time criteria (±5 days), but restrict the GOSAT measurements to those having a free-tropospheric temperature within ±2 K of that measured over the TCCON station. This allows averaging of measurements of air with similar dynamical origin. All GOSAT data that satisfy these criteria for a given day are averaged.

4 CarbonTracker

CarbonTracker release 2011 (Peters et al., 2007, http://carbontracker.noaa.gov/; henceforth CT2011) is an ensemble data assimilation scheme that uses surface, tower, and ship-borne in situ measurements of atmospheric CO_2 and the TM5 atmospheric transport model to produce 4-D fields of CO_2 (CarbonTracker, 2011). The TM5 model (Krol et al., 2005) is driven by the European Centre for Medium-range Weather Forecast (ECMWF) assimilated winds (Uppala et al., 2005; Molteni et al., 1996). There are four CO_2 flux "modules" embedded within CT2011: one for each of fire, fossil fuel, terrestrial biosphere, and ocean. These fluxes add to a background field to produce variability in assimilated CO_2. There are two priors for each of the fossil fuel, biosphere, and ocean flux modules, resulting in eight separate inversions, and the ensemble mean is reported as the result.

Only the terrestrial biosphere and ocean modules are optimized in the assimilation scheme: as with most assimilation schemes, the fire and fossil fuel fields are prescribed. The fire emissions are prescribed using the Global Fire Emissions Database (GFEDv3, CarbonTracker, 2011; Giglio et al., 2006; van der Werf et al., 2010; Mu et al., 2011). CT2011 assumes that the fossil fuel emissions are known from reported annual national and global inventories compiled by the Carbon Dioxide Information Analysis Center (CDIAC, Boden et al., 2011; CarbonTracker, 2011).

The terrestrial biosphere module in CT2011 is optimized based on priors from the monthly mean Carnegie-Ames-Stanford Approach (CASA) ecosystem exchange model (Potter et al., 1993; Randerson et al., 1997), which uses satellite measurements of the normalized difference vegetation index (NDVI) and fractional photosynthetically active radiation (fPAR) as proxies for plant phenology, and year-specific weather. Diurnal and synoptic variability in R_e is imposed through a Q_{10} relationship with surface air temperatures ($R_e \propto Q_{10}^{(T-T_0)/10}$), assuming a Q_{10} of 1.5 for respiration globally (CarbonTracker, 2011). The terrestrial biosphere fluxes and fire emissions described above were generated from the same versions of the CASA GFED model.

The ocean module optimizes prior fluxes provided by oceanic flux inversions (Jacobson et al., 2007), and measurements of partial pressure CO_2 in the ocean surface (Takahashi et al., 2009). The prior fluxes have a smooth trend, but no interannual variability. Any interannual variability in the optimized fluxes from the oceanic module of CT2011 is due to atmospheric surface winds interacting with the ocean surface, affecting the gas transfer efficiency. The magnitude of the interannual variability is small compared with the biosphere (CarbonTracker, 2011).

We use CT2011 output sampled at the locations of the TCCON stations in this study. We smooth the CO_2 profiles with the TCCON column averaging kernels and a priori profiles, using the Rodgers and Connor (2003) method, and integrate the smoothed profiles to produce daily CTX_{CO_2}. (Note that to compute total columns from the CO_2 profiles associated with the individual flux modules, no smoothing is applied: we simply integrate the CO_2 profiles to produce $CTX_{CO_2}^{module}$.)

This version of CarbonTracker has recently been replaced because of the discovery of a bug in the TM5 transport model. This bug is thought to have a negligible affect on the CO_2 mole fractions and no effect on fluxes from fossil fuel and wildfire emissions (CarbonTracker, 2011).

5 GEOS-Chem and SiB

GEOS-Chem is a global chemical transport model with CO_2 simulations described by Suntharalingam et al. (2003, 2004) and updated by Nassar et al. (2010). Typically, the CASA ecosystem exchange model is used to generate a priori biospheric CO_2 fluxes in GEOS-Chem. Messerschmidt et al. (2013) have recently shown that replacing CASA with the Simple Biosphere model (SiB3, Baker et al., 2008; Sellers et al., 1996a; Parazoo et al., 2008) significantly improves the CO_2 seasonal cycle amplitude and phase compared with TCCON observations. SiB3 calculates year-dependent fluxes using satellite measurements of plant phenology (Sellers et al., 1996b) yielding significant interannual variability in GPP (Baker et al., 2010). Here, phenological parameters are prescribed from the Moderate Resolution Imaging Spectroradiometer (MODIS, Zhao et al., 2006). Ecosystem respiration in SiB is driven by a Q_{10} relationship with surface air temperature (T), modified by a soil moisture term, $g(m)$ (Denning et al., 1996):

$$R_e = R_0 Q_{10}^{(T-298)/10} g(m). \quad (1)$$

The soil moisture term is defined in Denning et al. (1996, Eq. 8) and is related to the fraction of root zone soil porosity holding water, prescribed for each soil type by Raich et al. (1991). Based on the work of Raich and Schlesinger (1992), Q_{10} in SiB is set to 2.4.

Here, the GEOS-Chem model was run twice: once with SiB 2009 fluxes (referred to as "SiB 2009"), and once with year-dependent SiB fluxes (referred to simply as "SiB"). CO_2 profiles from the model are interpolated to the locations of the TCCON stations, smoothed with the TCCON column averaging kernels and a priori profiles, integrated, and then averaged to produce daily $SiBX_{CO_2}$.

Table 1. Mean annual CO_2 growth rates published on the ESRL-NOAA webpage: http://www.esrl.noaa.gov/gmd/ccgg/trends/global.html. The rates and their uncertainties are expressed in ppm yr^{-1}.

Year	Growth Rate (α)	Uncertainty
2000	1.25	0.10
2001	1.80	0.10
2002	2.38	0.07
2003	2.24	0.10
2004	1.61	0.05
2005	2.43	0.07
2006	1.74	0.06
2007	2.10	0.07
2008	1.80	0.05
2009	1.69	0.10
2010	2.41	0.06
2011	1.69	0.09
2012	2.77	0.09

6 Methods

To determine the seasonal cycle minimum date and value, we fit the measured X_{CO_2} and the CTX_{CO_2} time series with an annual periodic function superimposed on the Earth System Research Laboratory (ESRL) global annual CO_2 growth rate (Table 1, Conway and Tans, 2013). We do not assume the ESRL global annual growth rates for the GEOS-Chem time series; instead, we add an additional linear increase term (αx) to the fit. The fitted curves do not permit inter-annual variations in the seasonal cycle *shape*. The functional form of the fitted curve is a Fourier series:

$$f(x) = \sum_{k=0}^{2} a_k \cos(2\pi k x) + b_k \sin(2\pi k x), \quad (2)$$

where x is the fractional year (e.g., 14 August 2009 is 2009.62). The coefficients calculated for each time series are in Table 2. The date of the seasonal cycle minimum for each dataset is set by the local minimum in the fitted curves. Figure 1 shows the time series at Park Falls, Lamont, Białystok and Bremen measured by the TCCON instruments. Overlaid are the fitted curves for each time series. Figure 2 shows the time series detrended using the ESRL global annual growth rates, marking the date of the seasonal cycle minimum with symbols.

To assess how well the models compare with the TCCON data, we follow Yang et al. (2007) and use a least squares fit to find the amplitude and phase that minimizes differences between the seasonal cycles computed from the models and the TCCON data. Figure 3 shows the detrended seasonal cycles from the fitted curves (i.e., the $k = 1, 2$ terms from Eq. 2) to the models and the data. The agreement is generally good: the amplitudes of the $SiBX_{CO_2}$ seasonal cycles are too large

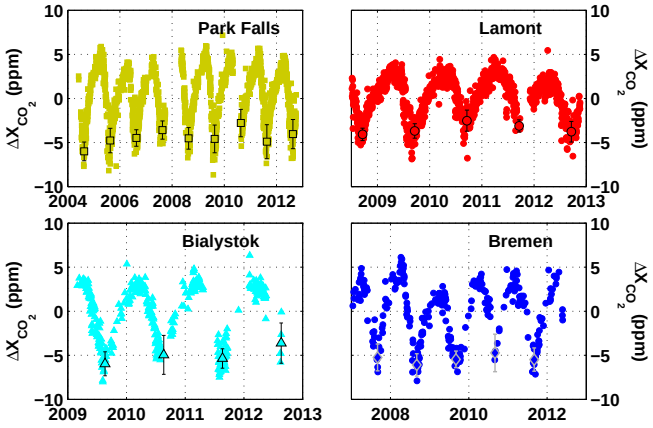

Fig. 2. The time series in Fig. 1 detrended to show the seasonal cycle in ΔX_{CO_2}. The symbols show the drawdown values and their 1σ error bars. The 2007 and 2010 ΔX_{CO_2} seasonal cycle minima are relatively weak compared with those in 2008 and 2009.

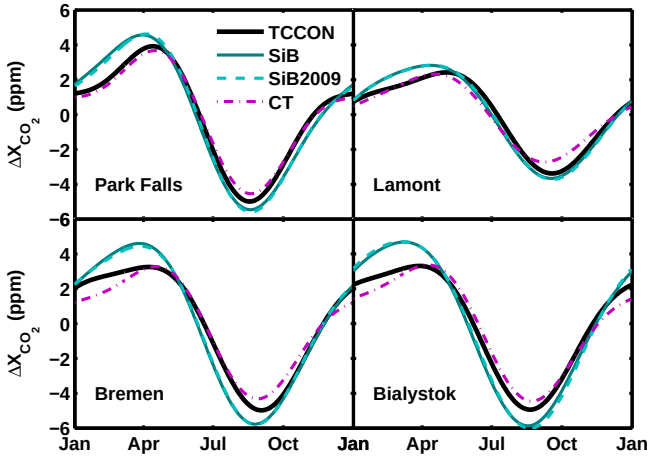

Fig. 3. Detrended seasonal cycles calculated by fitting the data and models (Eq. 2). Model seasonal cycles agree reasonably well with the TCCON data. See Table 3 for the amplitude ratios and time lags.

by ∼10–20 %, but show good agreement in the timing of the seasonal cycle (within 7 days). The amplitudes and time lags from the CTX_{CO_2} seasonal cycles match the TCCON data well, with the exception of an 8-day time lag at Lamont (Table 3).

The seasonal cycle minimum value (which we will call the "drawdown value") is determined by subtracting the fitted curves from the time series, and averaging the resulting ΔX_{CO_2} within ±15 days of the seasonal cycle minimum. The reported errors on the drawdown value represent the standard deviation (1σ) of the measurements. In years with fewer than 3 days of measurements near the seasonal cycle minimum, this averaging date range is extended to be within ±25 days (Białystok and Bremen data in 2010). The errors for these data points are tripled to reflect the additional uncertainty.

Table 2. Curve fitting parameters for Eq. (2). The parameters α and a_0 represent the linear secular increase: α is in ppm yr^{-1}, and a_0 is the y intercept in ppm. Parameter a_1 (ppm) represents the amplitude of the $\cos(2\pi x)$ term, and b_1 (ppm) represents the amplitude of the $\sin(2\pi x)$ term. The a_2 and b_2 parameters are the amplitudes of the $\cos(4\pi x)$ and $\sin(4\pi x)$ terms, respectively. The drawdown date (DD) and seasonal cycle maximum date (MD) are the dates of the local minima and maxima of the fitted curves, respectively, in day of the year. The large negative values of a_0 for SiB and SiB2009 are the result of using a straight-line fit to the data (i.e., α) instead of subtracting the ESRL growth curve, and fitting the detrended curve.

Site	α	a_0	a_1	a_2	b_1	b_2	DD	MD
Park Falls (TCCON)	ESRL (see Table 1)	0.97	1.70	−0.49	3.31	−1.45	230	104
Lamont (TCCON)	ESRL (see Table 1)	1.35	0.17	0.53	2.68	−0.53	261	123
Białystok (TCCON)	ESRL (see Table 1)	0.59	2.32	−0.11	3.21	−1.02	232	87
Bremen (TCCON)	ESRL (see Table 1)	1.35	1.64	0.40	3.63	−0.94	245	98
Park Falls (GOSAT)	ESRL (see Table 1)	0.70	0.95	−0.49	2.91	−1.15	232	106
Lamont (GOSAT)	ESRL (see Table 1)	0.97	0.22	0.32	2.45	−0.47	259	115
Białystok (GOSAT)	ESRL (see Table 1)	0.30	1.83	−0.31	3.09	−1.05	231	96
Bremen (GOSAT)	ESRL (see Table 1)	0.29	1.42	−0.14	2.89	−1.05	235	102
Park Falls (SiB)	2.22	−4075.59	2.25	−0.51	4.06	−1.00	231	90
Lamont (SiB)	2.29	−4217.89	0.47	0.35	3.15	−0.39	260	102
Białystok (SiB)	2.44	−4511.29	3.26	−0.25	4.05	−0.69	229	67
Bremen (SiB)	2.27	−4169.57	2.36	−0.15	4.42	−0.90	237	85
Park Falls (SiB 2009)	2.25	−4129.40	2.14	−0.51	4.11	−1.16	232	94
Lamont (SiB 2009)	2.31	−4260.74	0.40	0.40	3.19	−0.39	261	104
Białystok (SiB 2009)	2.40	−4438.20	3.27	−0.10	4.21	−0.72	232	65
Bremen (SiB 2009)	2.29	−4216.98	2.34	−0.07	4.35	−0.97	238	87
Park Falls (CT2011)	ESRL (see Table 1)	0.93	1.39	−0.41	3.09	−1.37	232	106
Lamont (CT2011)	ESRL (see Table 1)	1.33	0.37	0.10	2.32	−0.52	251	108
Białystok (CT2011)	ESRL (see Table 1)	1.13	1.61	−0.18	3.16	−1.03	235	98
Bremen (CT2011)	ESRL (see Table 1)	1.23	1.18	0.04	3.17	−1.10	241	107

Table 3. Time lag and amplitude adjustments necessary to best fit the TCCON data with the model fits. The time lag is in days, where a positive time lag means that the model should be delayed to best fit the TCCON data. The amplitude is multiplicative, so a value less than 1 means that the model amplitude should be reduced to best fit the TCCON data. See Fig. 3 for the related figure.

Site	SiB		CarbonTracker	
	Time Lag	Amplitude	Time Lag	Amplitude
Park Falls	2.5 ± 1.3	0.89 ± 0.01	-2.10 ± 1.16	1.09 ± 0.03
Lamont	4.8 ± 2.2	0.85 ± 0.02	8.40 ± 2.11	1.16 ± 0.05
Białystok	6.3 ± 3.2	0.79 ± 0.03	-5.96 ± 2.69	1.07 ± 0.05
Bremen	6.7 ± 4.3	0.81 ± 0.04	-0.11 ± 3.92	1.12 ± 0.08

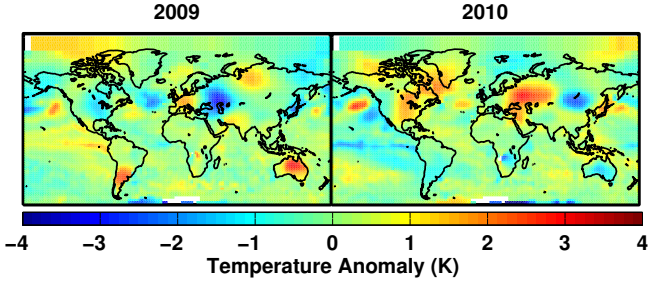

Fig. 4. The August surface temperature anomalies from GISS for 2009 (left) and 2010 (right) in degrees Kelvin. The Northern Hemisphere 2010 temperatures are significantly warmer than those in 2009.

To investigate the impact of the individual CT2011 modules (fires, fossil fuels, terrestrial biosphere, ocean) on the CTX_{CO_2} interannual variability, the fitting method described above (Eq. (2)) is not used, because the ESRL growth rate is only applicable to the total CO_2, and there may be no periodicity to some of the individual components. The $\Delta CTX_{CO_2}^{module}$ anomalies are instead computed by subtracting a yearly $\Delta CTX_{CO_2}^{module}$ mean that has been linearly interpolated to each time step. The drawdown values are the averages of these anomalies within ±15 days of the seasonal cycle minimum in total CTX_{CO_2}. The standard deviation of those values from year to year is then computed to estimate the interannual variability.

The calculated drawdown values are compared with August surface temperature measurements from the Goddard Institute for Space Science Surface Temperature Analysis (Hansen and Sato, 2004, http://data.giss.nasa.gov/gistemp/maps/). We use the 2004–2010 mean temperatures to compute surface temperature anomalies (ΔT) for years

2000–2012. The temperature anomalies are persistent: the July values and patterns are similar to August, and using 2000–2010 mean temperatures to compute anomalies results in negligible differences. Figure 4 shows the 2009 and 2010 August temperature anomalies as examples. As we wish to evaluate the coupling between the X_{CO_2} and the CO_2 fluxes, we weight the year-specific August surface temperature anomaly by the 2009 integrated growing season respiration from SiB (R_e^{2009GS}, in $kgC\,m^{-2}$) between 30° N and 60° N. These values are then divided by the 2009 integrated growing season (June, July, and August) ecosystem respiration between 30° N and 60° N to compute a respiration-weighted temperature anomaly, δT, for each year y. This weights the temperature anomalies more strongly in locations where the biosphere is active, and de-weights regions in which the biosphere is less active (i.e., over ocean, barren, or snow-covered areas).

$$\delta T_y = \frac{\sum_{j=180^\circ W}^{180^\circ E} \sum_{i=30^\circ N}^{60^\circ N} R_{e_{ij}}^{2009GS} \Delta T_{ij}^{y} \Delta a_{ij}}{\sum_{j=180^\circ W}^{180^\circ E} \sum_{i=30^\circ N}^{60^\circ N} R_{e_{ij}}^{2009GS} \Delta a_{ij}}, \quad (3)$$

where i is the latitude, j the longitude, and Δa_{ij} the grid area (in m^2). The value δT has units of temperature (K).

7 Results and discussion

Figure 2 shows the detrended X_{CO_2}, revealing clear interannual differences in the X_{CO_2} seasonal cycle minima that occur in summer to early autumn. The sites show similar patterns: 2007 and 2010 have relatively weak drawdowns, whereas 2008 and 2009 have relatively strong drawdowns. Surface temperature anomalies show that years 2007 and 2010 have relatively warm summertime midlatitudes, whereas 2008 and 2009 are relatively cool.

The correlation between the drawdown value and respiration-weighted temperature anomaly for Park Falls is plotted in Fig. 5, and the slopes ($\frac{\partial \Delta X_{CO_2}}{\partial \delta T}$) for all TCCON sites are listed in Table 4. The slopes for Park Falls, Białystok, Bremen and Lamont are consistent within their standard errors, giving a weighted average of $1.2 \pm 0.7\,ppm\,K^{-1}$. The Bremen slope is significantly smaller than the other slopes, possibly because of Bremen's proximity to urban fossil fuel emissions. Excluding Bremen from the weighted mean results in an average of $1.4 \pm 0.8\,ppm\,K^{-1}$. The Białystok slope is consistent with the Park Falls and Lamont slopes, but due to low data yields during the summers of 2010 and 2012, the error in the estimated slope is large. The standard errors are generally large at all sites because there is significant day-to-day variability in X_{CO_2} near the seasonal cycle minimum due to the influence of synoptic-scale activity on the measured X_{CO_2} (Keppel-Aleks et al., 2012). Figure 6 illustrates this increased summertime synoptic-scale "noise".

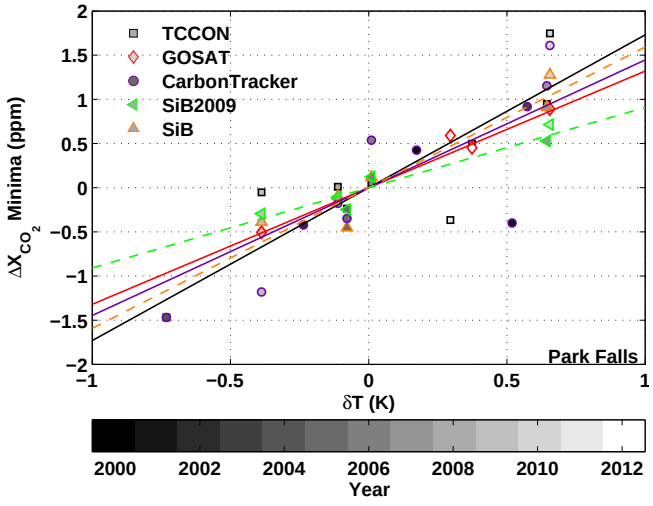

Fig. 5. The X_{CO_2} seasonal cycle minima at Park Falls are plotted against the respiration-weighted surface temperature anomalies from August. The TCCON data are shown in black-outlined squares, the GOSAT data in red diamonds, and the CarbonTracker2011 assimilation in purple circles. Each point represents a different year, with the grey shading denoting the year. The correspondingly colored solid lines are the best fits to the data points. The SiB model with year-specific biospheric parameters (SiB) and with a static 2009 biosphere (SiB 2009) are shown in orange and green triangles, respectively, with dashed best-fit lines. All best-fit lines are rescaled to cross zero on the y axis at zero δT.

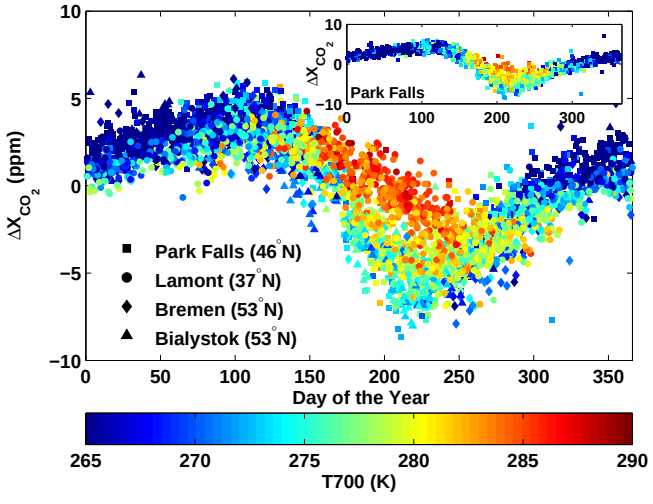

Fig. 6. Detrended X_{CO_2} seasonal cycles measured at the four TCCON stations. The colors are the free-troposphere temperatures (at 700 hPa, denoted T700). The color bar is scaled to emphasize the spring and summer months. The summertime ΔX_{CO_2} is lowest when the T700 values are coolest, and highest when the T700 values are warmest. The inset is Park Falls data alone, illustrating the increase in synoptic-scale "noise" in the summer.

Table 4. Slopes of $\Delta X_{CO_2} - \delta T$ relationship in ppm K^{-1} calculated from the TCCON measurements and the model runs. The errors are the standard errors on the linear fits. The respiration-weighted surface temperature (δT) are from August surface temperatures.

Site	TCCON	GOSAT	SiB	SiB 2009	CarbonTracker
Park Falls	1.73 ± 0.92	1.32 ± 1.43	1.59 ± 1.16	0.91 ± 1.13	1.45 ± 0.99
Lamont	1.10 ± 1.13	1.21 ± 0.83	1.18 ± 0.53	0.77 ± 0.53	0.92 ± 0.67
Bremen	0.42 ± 1.41	-0.36 ± 2.14	-0.11 ± 1.03	-0.40 ± 1.10	0.35 ± 0.71
Białystok	1.25 ± 2.06	-0.30 ± 1.78	0.71 ± 1.72	-0.05 ± 1.62	0.69 ± 0.70
Weighted Mean	1.19 ± 0.72	0.70 ± 0.81	0.91 ± 0.59	0.43 ± 0.58	0.81 ± 0.39
Weighted Mean without Bremen	1.41 ± 0.84	0.90 ± 0.81	1.21 ± 0.71	0.66 ± 0.68	0.97 ± 0.46

Table 5. The contribution of the four modules (fire, fossil fuel, terrestrial biosphere, and ocean) to the total interannual variability (IAV) in CT2011. The total IAV is the standard deviation of the drawdown period CTX_{CO_2} (in ppm), broken down into the fraction of that variability caused by the four modules (in percent).

Site	Total IAV (ppm)	Fires %	Fossil Fuel %	Biosphere %	Ocean %
Park Falls	0.90	6	10	82	3
Lamont	0.77	6	23	68	3
Bremen	0.48	13	22	60	5
Białystok	0.55	11	23	63	4

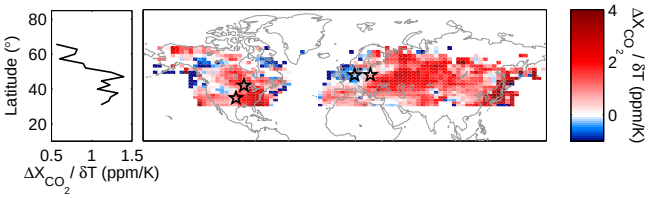

Fig. 7. A map of the mean $\Delta X_{CO_2} - \delta T$ slope over the 30–70° N region from two summertime drawdown periods using GOSAT data. The TCCON stations involved in this study are indicated with black stars. The panel on the left shows the zonal-mean $\Delta X_{CO_2} - \delta T$ slope as a function of latitude. Note that the latitude scales are not the same for the left panel and map: the left panel is linear in latitude, while the map is a Miller projection.

In the summertime, air that has originated from the north (cooler air) tends to have lower X_{CO_2} values, whereas air that originated from the south (warmer air) has higher X_{CO_2} values, giving rise to high variability in X_{CO_2} in the growing season. Covariations between the drawdown values and 30° N to 60° N surface temperatures (not weighted by R_e) show larger relative errors on the slopes, but consistent slope values (within error). Using the Mauna Loa growth rate instead of the global mean ESRL growth rate decreases the overall slopes by ~ 0.2 ppm K^{-1}.

The GOSAT slopes (0.7 ± 0.8 ppm K^{-1}) are consistent with the TCCON values within the errors. More revealing from the GOSAT analysis is the spatial distribution of the GOSAT slopes and their latitudinal gradient, which decreases from ~ 1.3 ppm K^{-1} near 30° N to ~ 0.7 ppm K^{-1} by 60° N (Fig. 7). The spatial pattern is mostly uniform, except near the oceans, and in regions of large local fossil fuel emissions (e.g., western Europe). This is consistent with our understanding that X_{CO_2} has a very large spatial footprint that is essentially hemispheric on seasonal timescales. The cause of the spatial variability near the coasts is unclear.

The significant correlation of X_{CO_2} with temperature could point to a large-scale dynamical effect, fires, fossil fuel use, or a biospheric reaction to the temperature changes. It is unlikely to be related to oceanic fluxes, as the interannual variability in CO_2 from ocean fluxes is negligible (Table 5). The possible contributing effects and an estimate of their relative importance are discussed in turn below.

7.1 Dynamics

Variability in the dynamical mixing of CO_2 within and between the midlatitudes and the tropics is expected to be correlated with surface temperature changes, since the meridional thermal structure both responds to and drives north–south transport of air (Trenberth, 1990; Webster, 1981). Therefore, it is plausible that the slopes seen in the TCCON and GOSAT data are influenced by interannual variability in the atmospheric mixing. To test this, we use the GEOS-Chem dynamical fields with static SiB 2009 biospheric fluxes, holding the NEE cycle constant from year to year. The results are shown in Fig. 5 for Park Falls, and in Table 4 for all sites. The SiB run with 2009 fluxes shows a weakly positive slope that is approximately 40 % of that observed, indicating that variability in the mixing does contribute to the observed interannual variability in X_{CO_2} minima. Because the covariations are computed with column-averaged CO_2, which is less influenced by local dynamics, this suggests that large-scale dynamics are important: warm years are associated with enhanced mixing of high CO_2 air from the subtropics with low CO_2 air from the Arctic, and weaker mixing in cool years.

7.2 Fires

High temperature (and lower humidity) conditions might be expected to be correlated with wild fire activity (e.g., Westerling et al., 2006) and therefore increased atmospheric CO_2 (Zhao and Running, 2010; Patra et al., 2005). To determine whether variations in fires have a significant effect on the

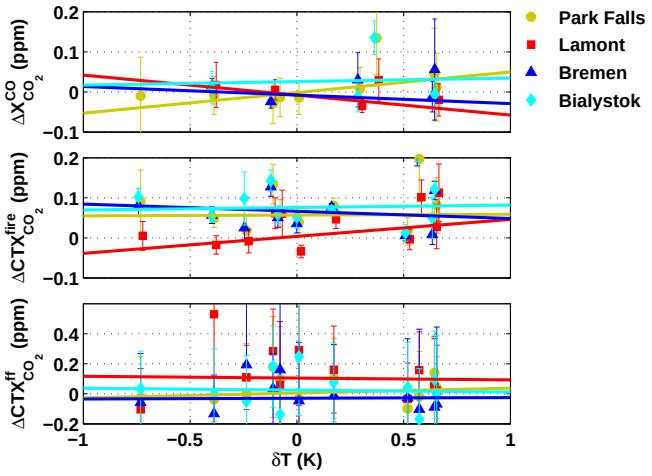

Fig. 8. The top panel shows the TCCON ΔX_{CO_2} calculated from measured ΔX_{CO} during the summertime drawdown against the respiration-weighted surface temperature, to probe the effects of forest fires on the ΔX_{CO_2}. The solid lines show the best-fit lines, which have very poor fit statistics ($R^2 < 0.2$). The middle panel shows the CT2011 fire contribution to the summertime drawdown in CTX_{CO_2}, which also has a negligible relationship with the respiration-weighted surface temperature. The bottom panel shows the CT2011 fossil fuel contribution to the summertime drawdown, which has a negligible relationship with the respiration-weighted surface temperature.

variations in X_{CO_2} seasonal cycle minima, we analyze TCCON measurements of X_{CO}, a fire tracer measured simultaneously with the X_{CO_2}. The anomalies in X_{CO} are calculated in an identical manner to X_{CO_2}, except that we do not use the ESRL CO_2 mean growth rate, but fit an additional linear increase parameter (αx). Following Akagi et al. (2011), we assume that the modified combustion efficiency of producing CO_2 from biomass burning is $\sim 88\,\%$ in the boreal forest, and we convert the measured ΔX_{CO} at the time of the X_{CO_2} drawdown into the ΔX_{CO_2} contribution from fires. We show the relationship between ΔX_{CO_2} caused by fires with the respiration-weighted temperature anomaly in Fig. 8. The variability in ΔX_{CO_2} caused by fires is at most $\sim 0.05\,\mathrm{ppm\,K^{-1}}$. Although CO is not a conserved tracer (its oxidation by OH leads to a lifetime of $\sim$1–2 months (Yurganov et al., 2004)), the small slope, even if a lower bound, suggests that fire does not contribute significantly to the observed $\sim 1.2\,\mathrm{ppm\,K^{-1}}$ variability.

Consistently, the CT2011 fire signature ($CTX^{fires}_{CO_2}$) accounts for only 6–13 % of the total interannual variability in summertime drawdown CTX_{CO_2} in CarbonTracker (see Table 5). The fire anomalies ($\Delta CTX^{fires}_{CO_2}$) have a weak relationship with the respiration-weighted temperature anomalies (Fig. 8), and a maximum slope of $\sim 0.05\,\mathrm{ppm\,K^{-1}}$.

7.3 Fossil fuel

The fossil fuel contribution ($CTX^{ff}_{CO_2}$) to the CTX_{CO_2} contains significant interannual variability ($\sim 23\,\%$ in Lamont, Bremen and Białystok, and $\sim 10\,\%$ in Park Falls, see Table 5). Because we detrend the TCCON data and CT2011 assimilation output of total X_{CO_2} by the annual measured CO_2 growth rate, some of the variability in the annual fossil fuel emissions will be removed from the ΔX_{CO_2} anomalies and will not contribute to the $\Delta X_{CO_2} - \delta T$ slope. Any remaining variability attributed to the fossil fuel signature is likely due partially to the dynamical effects described in Sect. 7.1, which would act to reduce the overall $\Delta X_{CO_2} - \delta T$ slopes, because fossil fuel emissions primarily occur in the northern midlatitudes, and are of opposite sign to the biospheric drawdown. If we assume that $\sim$2 PgC are emitted from fossil fuels in the Northern Hemisphere growing season, and that the growing season NEE represents a $\sim$5 Pg C sink, the fossil fuel emissions represent about one-third of the overall flux. If the dynamics produce about half of the temperature sensitivity, as we suggest in Sect. 7.1, then about one-sixth of the overall signal will be caused by the interaction of fossil fuel emissions and dynamics. This would produce a temperature sensitivity of $\sim 0.2\,\mathrm{ppm\,K^{-1}}$ on a hemispheric scale, which is significantly smaller than our uncertainties. The CT2011 fossil fuel signal ($CTX^{ff}_{CO_2}$) is not significantly correlated with the respiration-weighted surface temperature (Fig. 8, bottom panel), but is not inconsistent with a small, negative slope.

The impact of fossil fuel emissions on TCCON data may be largest in western Europe. Bremen has a much smaller $\Delta X_{CO_2} - \delta T$ relationship than most of the Northern Hemisphere in both the observations and models. This is a persistent feature of western Europe, which has consistently lower slopes than the rest of the northern midlatitudes (Fig. 7). Further, the rough difference between the Park Falls and Bremen slopes for both the TCCON results and the SiB2009 simulations is $\sim 1.3\,\mathrm{ppm\,K^{-1}}$, suggesting that this difference may reflect the large net efflux from western Europe.

7.4 NEE

The most significant contribution to interannual variability in CTX_{CO_2} is the terrestrial biosphere component, which accounts for 60 % in Bremen, increasing to 82 % in Park Falls (see Table 5). Respiration is directly influenced by surface temperature, and GPP is indirectly influenced by temperature through soil moisture. In SiB, both ecosystem respiration and GPP cause interannual variability in $SiBX_{CO_2}$. For example, the 2006 and 2009 $SiBX_{CO_2}$ seasonal cycle minima are similarly deep compared with 2010, and possess a similar growing season NEE. In 2006, the NEE was more negative relative to 2010 due to a decrease in respiration throughout the growing season. In contrast, in 2009, this was due to an increase in GPP relative to 2010. However, only the interannual variability in the integrated growing season ecosystem respiration is

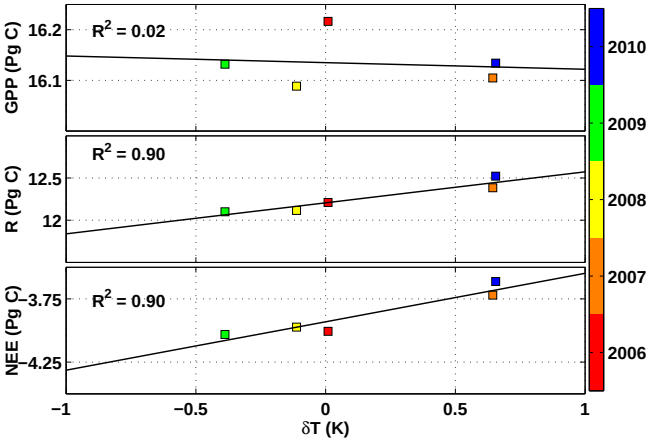

Fig. 9. The SiB 2006–2010 GPP (top), ecosystem respiration (middle), and NEE (bottom) integrated over the growing season (June, July and August) and over the northern midlatitudes (30° N to 60° N), plotted as a function of the respiration-weighted surface temperature anomaly. The colors indicate different years. The respiration and NEE fields have the most significant correlation with respiration-weighted temperature. The GPP does not have a significant correlation.

significantly correlated with the surface temperature anomalies ($R^2 \sim 0.9$, Fig. 9). The interannual variability in growing season GPP is not correlated with δT, suggesting that R_e is by far the stronger driver of this $\Delta X_{CO_2} - \delta T$ relationship in SiB. This is consistent with the results of Vukićević et al. (2003), who show that the temperature sensitivity of GPP is less than that of respiration in all versions of their model. However, "greenness" indices of plant phenology (such as NDVI) have been shown to be poor predictors of GPP in the boreal coniferous region in winter and during cloudy periods (Wang et al., 2004).

NEE depends on soil moisture through GPP and/or R_e (Raich et al., 1991; Denning et al., 1996; Zhao and Running, 2010), and so we evaluate soil moisture using the global gridded Palmer Drought Severity Index (PDSI, Dai et al., 2004; Dai, 2011a, b), which is available through 2010. PDSI values that are negative indicate dry conditions, and positive indices indicate wet conditions. Annual averages of PDSI from 30° N to 60° N weakly correlate with δT ($R^2 = 0.33$) for the years 2004–2010. However, it is difficult to determine whether the X_{CO_2} drawdown values from the TCCON measurements correlate significantly with PDSI. Only the Park Falls dataset has sufficient overlap with the available PDSI values, and it has a negative slope (drier conditions yield higher X_{CO_2} values). The other sites, even if they possess more than two years of coincident measurements, do not encompass a sufficiently large PDSI range to compute significant slopes.

8 Summary and future study

Interannual variability in the seasonal cycle minima of column-averaged dry-air mole fractions of CO_2 is correlated with summertime surface temperature anomalies in boreal regions. The CarbonTracker 2011 assimilation and GEOS-Chem simulations suggest that this relationship is caused both by dynamical mixing and biospheric activity, in roughly equal proportion. The effects of interannual variability in emissions from fossil fuel combustion and fires appear to be small and uncorrelated with surface temperature. However, dynamical effects on fossil fuel emissions should have an opposing effect on the $\Delta X_{CO_2} - \delta T$ relationship. The CT2011 and GEOS-Chem/SiB $\Delta X_{CO_2} - \delta T$ relationships are generally weaker than observed.

It is clear that there are several avenues worth pursuing to investigate further the processes responsible for the $\Delta X_{CO_2} - \delta T$ relationship. It is important to try other realizations of the dynamics: using different transport models such as TM5, or different underlying wind fields, such as ECMWF or NCEP. Because our results are derived from column-averaged atmospheric CO_2 measurements, which are relatively insensitive to planetary boundary layer (local) dynamics, we anticipate that differences in the large-scale dynamics will dominate the variability. A future investigation of the dynamical effects on fossil fuel emission-driven interannual variability should include a GEOS-Chem/SiB run with and without fossil fuel emissions in the model. We anticipate that, in the absence of fossil fuel emissions, the Bremen slopes would be similar to those measured elsewhere. The role of the oceans should be explored in more detail, including an assessment of the impacts of temperature variability and sea ice on gas exchange, and changes in ocean biogeochemistry associated with different climate modes.

To disentangle the effects of NEE on the observed variability further, both the effects of GPP and R_e should be probed. Although interannual variability in GPP is not correlated with δT in SiB, Guerlet et al. (2013) have attributed the interannual variability in the GOSAT 2009–2010 seasonal cycles to reduced carbon uptake (GPP) through their inversions. However, the 2010 Northern Hemisphere had exceptional warming, causing record-breaking heat waves throughout eastern Europe and Russia, and fires in western Russia (Barriopedro et al., 2011). The correlation between δT and GPP should be explored in other biospheric models, and by using chlorophyll fluorescence (e.g., Frankenberg et al., 2011) or $\delta^{18}O$ (e.g., Welp et al., 2011) instead of, or in conjunction with, the current proxies for plant phenology (e.g., NDVI). Further, the sensitivity of R_e to temperature (Q_{10}) and moisture should be studied further, through the use of $\delta^{13}C$ in situ measurements (e.g., Bowling et al., 2002) or other means.

Developing robust metrics for respiration and GPP responses to temperature is critical for reducing uncertainties in Earth system models and for diagnosing the vulnerability of permafrost carbon pools to future change.

Acknowledgements. The authors would like to thank Prof. Peter Rayner and an anonymous reviewer for helpful comments that substantially improved this paper. CarbonTracker 2011 results were provided by NOAA ESRL, Boulder, Colorado, USA, from the website at http://carbontracker.noaa.gov. US funding for TCCON comes from NASA's Carbon Cycle Program, grant number NNX11AG01G, the Orbiting Carbon Observatory Program, and the DOE/ARM Program. We acknowledge financial support of the Białystok TCCON site from the Senate of Bremen and EU projects IMECC and GEOmon as well as maintenance and logistical work provided by AeroMeteo Service. P. O. Wennberg and J. T. Randerson receive support from NASA's Carbon Cycle Science program (NNX10AT83G). The GOSAT X_{CO_2} data were obtained from the Atmospheric CO_2 Observations from Space (ACOS) project. We thank the three Japanese parties (NIES, JAXA, MOE) for making the GOSAT spectra available to the scientific community. N. C. Parazoo carried out the research at the University of California Los Angeles and the Jet Propulsion Laboratory, and acknowledges support from NASA ROSES NNH09ZDA001N-ACOS. Part of this work was performed at the Jet Propulsion Laboratory, California Institute of Technology, under contract with NASA. Self-calibrated PDSI data with Penman–Monteith PE were downloaded from http://www.cgd.ucar.edu/cas/catalog/climind/pdsi.html.

Edited by: I. Aben

References

Akagi, S. K., Yokelson, R. J., Wiedinmyer, C., Alvarado, M. J., Reid, J. S., Karl, T., Crounse, J. D., and Wennberg, P. O.: Emission factors for open and domestic biomass burning for use in atmospheric models, Atmos. Chem. Phys., 11, 4039–4072, doi:10.5194/acp-11-4039-2011, 2011.

Arnone, J. A., Verburg, P. S. J., Johnson, D. W., Larsen, J. D., Jasoni, R. L., Lucchesi, A. J., Batts, C. M., von Nagy, C., Coulombe, W. G., Schorran, D. E., Buck, P. E., Braswell, B. H., Coleman, J. S., Sherry, R. A, Wallace, L. L., Luo, Y. and Schimel, D. S.: Prolonged suppression of ecosystem carbon dioxide uptake after an anomalously warm year., Nature, 455, 383–386, doi:10.1038/nature07296, 2008.

Baker, I. T., Prihodko, L., Denning, A. S., Goulden, M., Miller, S., and da Rocha, H. R.: Seasonal drought stress in the Amazon: reconciling models and observations, J. Geophys. Res., 113, G00B01, doi:10.1029/2007JG000644, 2008.

Baker, I. T., Denning, A. S., and Stöckli, R.: North American gross primary productivity: regional characterization and interannual variability, Tellus B, 62, 533–549, doi:10.1111/j.1600-0889.2010.00492.x, 2010.

Barriopedro, D., Fischer, E. M., Luterbacher, J., Trigo, R. M., and García-Herrera, R.: The hot summer of 2010: redrawing the temperature record map of Europe, Science, 332, 220–224, doi:10.1126/science.1201224, 2011.

Boden, T. A., Marland, G., and Andres, R. J.: Global, Regional, and National Fossil-Fuel CO_2 Emissions, Carbon Dioxide Information Analysis Center, Oak Ridge National Laboratory, US Department of Energy, Oak Ridge, Tenn., USA, doi:10.3334/CDIAC/00001_V2011, 2011.

Bowling, D., McDowell, N., Bond, B., Law, B., and Ehleringer, J.: ^{13}C content of ecosystem respiration is linked to precipitation and vapor pressure deficit, Oecologia, 131, 113–124, doi:10.1007/s00442-001-0851-y, 2002.

Braswell, B. H., Schimel, D. S., Linder, E., and Moore, B.: The response of global terrestrial ecosystems to interannual temperature variability, Science, 278, 870–873, doi:10.1126/science.278.5339.870, 1997.

CarbonTracker: Documentation – CT2011, Tech. rep., Earth System Research Laboratory – National Oceanic and Atmospheric Administration, available at: http://www.esrl.noaa.gov/gmd/ccgg/carbontracker/documentation_obs.html, 2011.

Conway, T. and Tans, P.: Annual mean global carbon dioxide growth rates, available at: http://www.esrl.noaa.gov/gmd/ccgg/trends/global.html, NOAA/ESRL, last access: 7 January 2013.

Cox, P. M., Pearson, D., Booth, B. B., Friedlingstein, P., Huntingford, C., Jones, C. D., and Luke, C. M.: Sensitivity of tropical carbon to climate change constrained by carbon dioxide variability., Nature, 494, 341–344, doi:10.1038/nature11882, 2013.

Crisp, D., Fisher, B. M., O'Dell, C., Frankenberg, C., Basilio, R., Bösch, H., Brown, L. R., Castano, R., Connor, B., Deutscher, N. M., Eldering, A., Griffith, D., Gunson, M., Kuze, A., Mandrake, L., McDuffie, J., Messerschmidt, J., Miller, C. E., Morino, I., Natraj, V., Notholt, J., O'Brien, D. M., Oyafuso, F., Polonsky, I., Robinson, J., Salawitch, R., Sherlock, V., Smyth, M., Suto, H., Taylor, T. E., Thompson, D. R., Wennberg, P. O., Wunch, D., and Yung, Y. L.: The ACOS CO_2 retrieval algorithm – Part II: Global X_CO_2 data characterization, Atmos. Meas. Tech., 5, 687–707, doi:10.5194/amt-5-687-2012, 2012.

Dai, A.: Characteristics and trends in various forms of the Palmer Drought Severity Index during 1900–2008, J. Geophys. Res., 116, D12115, doi:10.1029/2010JD015541, 2011a.

Dai, A.: Drought under global warming: a review, Wiley Interdisciplinary Reviews, Climate Change, 2, 45–65, doi:10.1002/wcc.81, 2011b.

Dai, A., Trenberth, K. E., and Qian, T.: A global dataset of Palmer Drought Severity Index for 1870–2002: relationship with soil moisture and effects of surface warming, J. Hydrometeorol., 5, 1117–1130, doi:10.1175/JHM-386.1, 2004.

D'Arrigo, R., Jacoby, G. C., and Fung, I. Y.: Boreal forests and atmosphere-biosphere exchange of carbon dioxide, Nature, 329, 321–323, doi:10.1038/329321a0, 1987.

Denning, A. S., Collatz, G. J., Zhang, C., Randall, D. A., Berry, J. A., Sellers, P. J., Colello, G. D., and Dazlich, D. A.: Simulations of terrestrial carbon metabolism and atmospheric CO_2 in a general circulation model, Part 1: Surface carbon fluxes, Tellus B, 48, 521–542, doi:10.1034/j.1600-0889.1996.t01-2-00009.x, 1996.

Doughty, C. E. and Goulden, M. L.: Are tropical forests near a high temperature threshold?, J. Geophys. Res., 113, G00B07, doi:10.1029/2007JG000632, 2008.

Francey, R. J., Tans, P. P., Allison, C. E., Enting, I. G., White, J. W. C., and Trolier, M.: Changes in oceanic and

terrestrial carbon uptake since 1982, Nature, 373, 326–330, doi:10.1038/373326a0, 1995.

Frankenberg, C., Fisher, J. B., Worden, J., Badgley, G., Saatchi, S. S., Lee, J.-E., Toon, G. C., Butz, A., Jung, M., Kuze, A., and Yokota, T.: New global observations of the terrestrial carbon cycle from GOSAT: patterns of plant fluorescence with gross primary productivity, Geophys. Res. Lett., 38, 1–6, doi:10.1029/2011GL048738, 2011.

Fung, I. Y., Tucker, C. J., and Prentice, K. C.: Application of advanced very high resolution radiometer vegetation index to study atmosphere–biosphere exchange of CO_2, J. Geophys. Res., 92, 2999–3015, doi:10.1029/JD092iD03p02999, 1987.

Giglio, L., van der Werf, G. R., Randerson, J. T., Collatz, G. J., and Kasibhatla, P.: Global estimation of burned area using MODIS active fire observations, Atmos. Chem. Phys., 6, 957–974, doi:10.5194/acp-6-957-2006, 2006.

Guerlet S., S. Basu, A. Butz, M. Krol, P. Hahne, S. Houweling, O. P. Hasekamp, and I. Aben (2013), Reduced carbon uptake during the 2010 Northern Hemisphere summer from GOSAT, Geophys. Res. Lett., 40, 2378–2383, doi:10.1002/grl.50402, 2013.

Hamazaki, T.: Fourier transform spectrometer for Greenhouse Gases Observing Satellite (GOSAT), P. SPIE Is. T. Elect., 5659, 73–80, doi:10.1117/12.581198, 2005.

Hansen, J. and Sato, M.: Greenhouse gas growth rates., P. Natl. Acad. Sci. USA, 101, 16109–16114, doi:10.1073/pnas.0406982101, 2004.

Jacobson, A. R., Mikaloff Fletcher, S. E., Gruber, N., Sarmiento, J. L., and Gloor, M.: A joint atmosphere-ocean inversion for surface fluxes of carbon dioxide: 1. Methods and global-scale fluxes, Global Biogeochem. Cy., 21, GB1019, doi:10.1029/2005GB002556, 2007.

Keeling, C. D., Chin, J. F. S., and Whorf, T. P.: Increased activity of northern vegetation inferred from atmospheric CO_2 measurements, Nature, 382, 146–149, doi:10.1038/382146a0, 1996.

Keppel-Aleks, G., Wennberg, P. O., and Schneider, T.: Sources of variations in total column carbon dioxide, Atmos. Chem. Phys., 11, 3581–3593, doi:10.5194/acp-11-3581-2011, 2011.

Keppel-Aleks, G., Wennberg, P. O., Washenfelder, R. A., Wunch, D., Schneider, T., Toon, G. C., Andres, R. J., Blavier, J.-F., Connor, B., Davis, K. J., Desai, A. R., Messerschmidt, J., Notholt, J., Roehl, C. M., Sherlock, V., Stephens, B. B., Vay, S. A., and Wofsy, S. C.: The imprint of surface fluxes and transport on variations in total column carbon dioxide, Biogeosciences, 9, 875–891, doi:10.5194/bg-9-875-2012, 2012.

Keppel-Aleks, G., Randerson, J. T., Lindsay, K., Stephens, B. B., Moore, J. K., Doney, S. C., Thornton, P. E., Mahowald, N. M., Hoffman, F. M., Sweeney, C., Tans, P. P.,Wennberg, P. O., and Wofsy, S. C.: Atmospheric 460 carbon dioxide variability in the Community Earth System Model: evaluation and transient dynamics during the 20th and 21st centuries, J. Climate, 26, 4447–4475, doi:10.1175/JCLI-D-12-00589.1, 2013.

Krol, M., Houweling, S., Bregman, B., van den Broek, M., Segers, A., van Velthoven, P., Peters, W., Dentener, F., and Bergamaschi, P.: The two-way nested global chemistry-transport zoom model TM5: algorithm and applications, Atmos. Chem. Phys., 5, 417–432, doi:10.5194/acp-5-417-2005, 2005.

Langenfelds, R. L., Francey, R. J., Pak, B. C., Steele, L. P., Lloyd, J., Trudinger, C. M., and Allison, C. E.: Interannual growth rate variations of atmospheric CO_2 and its ^{13}C, H_2, CH_4, and CO between 1992 and 1999 linked to biomass burning, Global Biogeochem. Cy., 16, 1–22, doi:10.1029/2001GB001466, 2002.

Lloyd, J. and Taylor, J. A.: On the temperature dependence of soil respiration, Funct. Ecol., 8, 315, doi:10.2307/2389824, 1994.

Machta, L.: Mauna Loa and global trends in air quality, B. Am. Meteorol. Soc., 53, 402–420, doi:10.1175/1520-0477(1972)053<0402:MLAGTI>2.0.CO;2, 1972.

Messerschmidt, J., Geibel, M. C., Blumenstock, T., Chen, H., Deutscher, N. M., Engel, A., Feist, D. G., Gerbig, C., Gisi, M., Hase, F., Katrynski, K., Kolle, O., Lavrič, J. V., Notholt, J., Palm, M., Ramonet, M., Rettinger, M., Schmidt, M., Sussmann, R., Toon, G. C., Truong, F., Warneke, T., Wennberg, P. O., Wunch, D., and Xueref-Remy, I.: Calibration of TCCON column-averaged CO_2: the first aircraft campaign over European TCCON sites, Atmos. Chem. Phys., 11, 10765–10777, doi:10.5194/acp-11-10765-2011, 2011.

Messerschmidt, J., Chen, H., Deutscher, N. M., Gerbig, C., Grupe, P., Katrynski, K., Koch, F.-T., Lavrič, J. V., Notholt, J., Rödenbeck, C., Ruhe, W., Warneke, T., and Weinzierl, C.: Automated ground-based remote sensing measurements of greenhouse gases at the Białystok site in comparison with collocated in situ measurements and model data, Atmos. Chem. Phys., 12, 6741–6755, doi:10.5194/acp-12-6741-2012, 2012a.

Messerschmidt, J., Parazoo, N., Wunch, D., Deutscher, N. M., Roehl, C., Warneke, T., and Wennberg, P. O.: Evaluation of seasonal atmosphere-biosphere exchange estimations with TCCON measurements, Atmos. Chem. Phys., 13, 5103–5115, doi:10.5194/acp-13-5103-2013, 2013.

Molteni, F., Buizza, R., Palmer, T. N., and Petroliagis, T.: The ECMWF ensemble prediction system: methodology and validation, Q. J. Roy. Meteor. Soc., 122, 73–119, doi:10.1002/qj.49712252905, 1996.

Mu, M., Randerson, J. T., van der Werf, G. R., Giglio, L., Kasibhatla, P., Morton, D., Collatz, G. J., DeFries, R. S., Hyer, E. J., Prins, E. M., Griffith, D. W. T., Wunch, D., Toon, G. C., Sherlock, V., and Wennberg, P. O.: Daily and 3-hourly variability in global fire emissions and consequences for atmospheric model predictions of carbon monoxide, J. Geophys. Res., 116, D24303, doi:10.1029/2011JD016245, 2011.

Nassar, R., Jones, D. B. A., Suntharalingam, P., Chen, J. M., Andres, R. J., Wecht, K. J., Yantosca, R. M., Kulawik, S. S., Bowman, K. W., Worden, J. R., Machida, T., and Matsueda, H.: Modeling global atmospheric CO_2 with improved emission inventories and CO_2 production from the oxidation of other carbon species, Geosci. Model Dev., 3, 689–716, doi:10.5194/gmd-3-689-2010, 2010.

O'Dell, C. W., Connor, B., Bösch, H., O'Brien, D., Frankenberg, C., Castano, R., Christi, M., Eldering, D., Fisher, B., Gunson, M., McDuffie, J., Miller, C. E., Natraj, V., Oyafuso, F., Polonsky, I., Smyth, M., Taylor, T., Toon, G. C., Wennberg, P. O., and Wunch, D.: The ACOS CO_2 retrieval algorithm – Part 1: Description and validation against synthetic observations, Atmos. Meas. Tech., 5, 99–121, doi:10.5194/amt-5-99-2012, 2012.

Parazoo, N. C., Denning, A. S., Kawa, S. R., Corbin, K. D., Lokupitiya, R. S., and Baker, I. T.: Mechanisms for synoptic variations of atmospheric CO_2 in North America, South America and Europe, Atmos. Chem. Phys., 8, 7239–7254, doi:10.5194/acp-8-7239-2008, 2008.

Patra, P. K., Ishizawa, M., Maksyutov, S., Nakazawa, T., and Inoue, G.: Role of biomass burning and climate anomalies for land-atmosphere carbon fluxes based on inverse modeling of atmospheric CO_2, Global Biogeochemical Cycles, 19(3), GB3005, doi:10.1029/2004GB002258, 2005.

Peters, W., Jacobson, A. R., Sweeney, C., Andrews, A. E., Conway, T. J., Masarie, K., Miller, J. B., Bruhwiler, L. M. P., Pétron, G., Hirsch, A. I., Worthy, D. E. J., van der Werf, G. R., Randerson, J. T., Wennberg, P. O., Krol, M. C., and Tans, P. P.: An atmospheric perspective on North American carbon dioxide exchange: CarbonTracker, P. Natl. Acad. Sci. USA, 104, 18925–18930, doi:10.1073/pnas.0708986104, 2007.

Piao, S., Ciais, P., Friedlingstein, P., Peylin, P., Reichstein, M., Luyssaert, S., Margolis, H., Fang, J., Barr, A., Chen, A., Grelle, A., Hollinger, D. Y., Laurila, T., Lindroth, A., Richardson, A. D., and Vesala, T.: Net carbon dioxide losses of northern ecosystems in response to autumn warming, Nature, 451, 49–52, doi:10.1038/nature06444, 2008.

Potter, C. S., Randerson, J. T., Field, C. B., Matson, P. A., Vitousek, P. M., Mooney, H. A., and Klooster, S. A.: Terrestrial ecosystem production: a process model based on global satellite and surface data, Global Biogeochem. Cy., 7, 811, doi:10.1029/93GB02725, 1993.

Raich, J. W. and Schlesinger, W. H.: The global carbon dioxide flux in soil respiration and its relationship to vegetation and climate, Tellus B, 44, 81–99, doi:10.3402/tellusb.v44i2.15428, 1992.

Raich, J. W., Rastetter, E. B., Melillo, J. M., Kicklighter, D. W., Steudler, P. A., Peterson, B. J., Grace III, A. L.,, B. M., and Vorosmarty, C. J.: Potential net primary productivity in South America: application of a global model, Ecol. Appl., 1, 399, doi:10.2307/1941899, 1991.

Randerson, J. T., Thompson, M. V., Conway, T. J., Fung, I. Y., and Field, C. B.: The contribution of terrestrial sources and sinks to trends in the seasonal cycle of atmospheric carbon dioxide, Global Biogeochem. Cy., 11, 535–560, doi:10.1029/97GB02268, 1997.

Randerson, J. T., Field, C. B., Fung, I. Y., and Tans, P. P.: Increases in early season ecosystem uptake explain recent changes in the seasonal cycle of atmospheric CO_2 at high northern latitudes, Geophys. Res. Lett., 26, 2765, doi:10.1029/1999GL900500, 1999.

Rayner, P. J., Enting, I. G., Francey, R. J., and Langenfelds, R.: Reconstructing the recent carbon cycle from atmospheric CO_2, ^{13}C and O_2/N_2 observations, Tellus B, 51, 213–232, doi:10.1034/j.1600-0889.1999.t01-1-00008.x, 1999.

Richardson, A. D., Hollinger, D. Y., Aber, J. D., Ollinger, S. V. and Braswell, B. H.: Environmental variation is directly responsible for short- but not long-term variation in forest-atmosphere carbon exchange, Global Change Biology, 13, 788–803, doi:10.1111/j.1365-2486.2007.01330.x, 2007.

Rodgers, C. D. and Connor, B. J.: Intercomparison of remote sounding instruments, J. Geophys. Res., 108, 4116, doi:10.1029/2002JD002299, 2003.

Sacks, W. J., Schimel, D. S., and Monson, R. K.: Coupling between carbon cycling and climate in a high-elevation, subalpine forest: a model-data fusion analysis., Oecologia, 151, 54–68, doi:10.1007/s00442-006-0565-2, 2007.

Sellers, P., Randall, D., Collatz, G., Berry, J., Field, C., Dazlich, D., Zhang, C., Collelo, G., and Bounoua, L.: A revised land surface parameterization (SiB2) for atmospheric GCMS, Part I: Model formulation, J. Climate, 9, 676–705, doi:10.1175/1520-0442(1996)009<0676:ARLSPF>2.0.CO;2, 1996a.

Sellers, P. J., Tucker, C. J., Collatz, G. J., Los, S. O., Justice, C. O., Dazlich, D. A., and Randall, D. A.: A revised land surface parameterization (SiB2) for atmospheric GCMS, Part II: The generation of global fields of terrestrial biophysical parameters from satellite data, J. Climate, 9, 706–737, doi:10.1175/1520-0442(1996)009<0706:ARLSPF>2.0.CO;2, 1996b.

Suntharalingam, P., Spivakovsky, C. M., Logan, J. A., and McElroy, M. B.: Estimating the distribution of terrestrial CO_2 sources and sinks from atmospheric measurements: sensitivity to configuration of the observation network, J. Geophys. Res., 108, 4452, doi:10.1029/2002JD002207, 2003.

Suntharalingam, P., Jacob, D. J., Palmer, P. I., Logan, J. A., Yantosca, R. M., Xiao, Y., Evans, M. J., Streets, D. G., Vay, S. L., and Sachse, G. W.: Improved quantification of Chinese carbon fluxes using CO_2/CO correlations in Asian outflow, J. Geophys. Res., 109, D18S18, doi:10.1029/2003JD004362, 2004.

Takahashi, T., Sutherland, S. C., Wanninkhof, R., Sweeney, C., Feely, R. a., Chipman, D. W., Hales, B., Friederich, G., Chavez, F., Sabine, C., Watson, A., Bakker, D. C., Schuster, U., Metzl, N., Yoshikawa-Inoue, H., Ishii, M., Midorikawa, T., Nojiri, Y., Körtzinger, A., Steinhoff, T., Hoppema, M., Olafsson, J., Arnarson, T. S., Tilbrook, B., Johannessen, T., Olsen, A., Bellerby, R., Wong, C., Delille, B., Bates, N., and de Baar, H. J.: Climatological mean and decadal change in surface ocean pCO_2, and net sea-air CO_2 flux over the global oceans, Deep Sea Res. Pt. II, 56, 554–577, doi:10.1016/j.dsr2.2008.12.009, 2009.

Trenberth, K. E.: Recent observed interdecadal climate changes in the Northern Hemisphere, B. Am. Meteor. Soc., 71, 988–993, doi:10.1175/1520-0477(1990)071<0988:ROICCI>2.0.CO;2, 1990.

Uppala, S. M., Kållberg, P. W., Simmons, A. J., Andrae, U., Bechtold, V. D. C., Fiorino, M., Gibson, J. K., Haseler, J., Hernandez, A., Kelly, G. A., Li, X., Onogi, K., Saarinen, S., Sokka, N., Allan, R. P., Andersson, E., Arpe, K., Balmaseda, M. A., Beljaars, A. C. M., Berg, L. V. D., Bidlot, J., Bormann, N., Caires, S., Chevallier, F., Dethof, A., Dragosavac, M., Fisher, M., Fuentes, M., Hagemann, S., Hólm, E., Hoskins, B. J., Isaksen, L., Janssen, P. A. E. M., Jenne, R., Mcnally, A. P., Mahfouf, J.-F., Morcrette, J.-J., Rayner, N. A., Saunders, R. W., Simon, P., Sterl, A., Trenberth, K. E., Untch, A., Vasiljevic, D., Viterbo, P., and Woollen, J.: The ERA-40 re-analysis, Q. J. Roy. Meteor. Soc., 131, 2961–3012, doi:10.1256/qj.04.176, 2005.

van der Werf, G. R., Randerson, J. T., Giglio, L., Collatz, G. J., Mu, M., Kasibhatla, P. S., Morton, D. C., DeFries, R. S., Jin, Y., and van Leeuwen, T. T.: Global fire emissions and the contribution of deforestation, savanna, forest, agricultural, and peat fires (1997–2009), Atmos. Chem. Phys., 10, 11707–11735, doi:10.5194/acp-10-11707-2010, 2010.

Vukićević, T., Braswell, B., and Schimel, D.: A diagnostic study of temperature controls on global terrestrial carbon exchange, Tellus B, 53, 150–170, doi:10.1034/j.1600-0889.2001.d01-13.x, 2003.

Wang, Q., Tenhunen, J., Dinh, N. Q., Reichstein, M., Vesala, T., and Keronen, P.: Similarities in ground- and satellite-based NDVI time series and their relationship to physiological activity of

a Scots pine forest in Finland, Remote Sens. Environ., 93, 225–237, doi:10.1016/j.rse.2004.07.006, 2004.

Washenfelder, R. A., Toon, G. C., Blavier, J.-F. L., Yang, Z., Allen, N. T., Wennberg, P. O., Vay, S. a., Matross, D. M., and Daube, B. C.: Carbon dioxide column abundances at the Wisconsin Tall Tower site, J. Geophys. Res., 111, 1–11, doi:10.1029/2006JD007154, 2006.

Webster, P. J.: Mechanisms determining the atmospheric response to sea surface temperature anomalies, J. Atmos. Sci., 38, 554–571, doi:10.1175/1520-0469(1981)038<0554:MDTART>2.0.CO;2, 1981.

Welp, L. R., Keeling, R. F., Meijer, H. A. J., Bollenbacher, A. F., Piper, S. C., Yoshimura, K., Francey, R. J., Allison, C. E., and Wahlen, M.: Interannual variability in the oxygen isotopes of atmospheric CO_2 driven by El Niño, Nature, 477, 579–582, doi:10.1038/nature10421, 2011.

Westerling, A. L., Hidalgo, H. G., Cayan, D. R., and Swetnam, T. W.: Warming and earlier spring increase western US forest wildfire activity, Science, 313, 940–943, doi:10.1126/science.1128834, 2006.

Wunch, D., Toon, G. C., Wennberg, P. O., Wofsy, S. C., Stephens, B. B., Fischer, M. L., Uchino, O., Abshire, J. B., Bernath, P., Biraud, S. C., Blavier, J.-F. L., Boone, C., Bowman, K. P., Browell, E. V., Campos, T., Connor, B. J., Daube, B. C., Deutscher, N. M., Diao, M., Elkins, J. W., Gerbig, C., Gottlieb, E., Griffith, D. W. T., Hurst, D. F., Jiménez, R., Keppel-Aleks, G., Kort, E. A., Macatangay, R., Machida, T., Matsueda, H., Moore, F., Morino, I., Park, S., Robinson, J., Roehl, C. M., Sawa, Y., Sherlock, V., Sweeney, C., Tanaka, T., and Zondlo, M. A.: Calibration of the Total Carbon Column Observing Network using aircraft profile data, Atmos. Meas. Tech., 3, 1351–1362, doi:10.5194/amt-3-1351-2010, 2010.

Wunch, D., Toon, G. C., Blavier, J.-F. L., Washenfelder, R. A., Notholt, J., Connor, B. J., Griffith, D. W. T., Sherlock, V., and Wennberg, P. O.: The total carbon column observing network, Philos. T. R. Soc. A, 369, 2087–2112, doi:10.1098/rsta.2010.0240, 2011a.

Wunch, D., Wennberg, P. O., Toon, G. C., Connor, B. J., Fisher, B., Osterman, G. B., Frankenberg, C., Mandrake, L., O'Dell, C., Ahonen, P., Biraud, S. C., Castano, R., Cressie, N., Crisp, D., Deutscher, N. M., Eldering, A., Fisher, M. L., Griffith, D. W. T., Gunson, M., Heikkinen, P., Keppel-Aleks, G., Kyrö, E., Lindenmaier, R., Macatangay, R., Mendonca, J., Messerschmidt, J., Miller, C. E., Morino, I., Notholt, J., Oyafuso, F. A., Rettinger, M., Robinson, J., Roehl, C. M., Salawitch, R. J., Sherlock, V., Strong, K., Sussmann, R., Tanaka, T., Thompson, D. R., Uchino, O., Warneke, T., and Wofsy, S. C.: A method for evaluating bias in global measurements of CO_2 total columns from space, Atmos. Chem. Phys., 11, 12317–12337, doi:10.5194/acp-11-12317-2011, 2011b.

Yang, Z., Washenfelder, R. A., Keppel-Aleks, G., Krakauer, N. Y., Randerson, J. T., Tans, P. P., Sweeney, C., and Wennberg, P. O.: New constraints on Northern Hemisphere growing season net flux, Geophys. Res. Lett., 34, L12807, doi:10.1029/2007GL029742, 2007.

Yokota, T., Yoshida, Y., Eguchi, N., Ota, Y., Tanaka, T., Watanabe, H., and Maksyutov, S.: Global concentrations of CO_2 and CH_4 retrieved from GOSAT: first preliminary results, Sola, 5, 160–163, doi:10.2151/sola.2009-041, 2009.

Yurganov, L. N., Blumenstock, T., Grechko, E. I., Hase, F., Hyer, E. J., Kasischke, E. S., Koike, M., Kondo, Y., Kramer, I., Leung, F.-Y., Mahieu, E., Mellqvist, J., Notholt, J., Novelli, P. C., Rinsland, C. P., Scheel, H. E., Schultz, A., Strandberg, A., Sussmann, R., Tanimoto, H., Velazco, V., Zander, R., and Zhao, Y.: A quantitative assessment of the 1998 carbon monoxide emission anomaly in the Northern Hemisphere based on total column and surface concentration measurements, J. Geophys. Res., 109, D15305, doi:10.1029/2004JD004559, 2004.

Zhao, M. and Running, S. W.: Drought-induced reduction in global terrestrial net primary production from 2000 through 2009, Science, 329, 940–943, doi:10.1126/science.1192666, 2010.

Zhao, M., Running, S. W., and Nemani, R. R.: Sensitivity of Moderate Resolution Imaging Spectroradiometer (MODIS) terrestrial primary production to the accuracy of meteorological reanalyses, J. Geophys. Res., 111, G01002, doi:10.1029/2004JG000004, 2006.